# A Fully Integrated 263-GHz Retro-Backscatter Circuit with 105°/82° Reading Angle and 12-dB Conversion Loss

Mingran Jia, Jinchen Wang, Jaehong Jung, Xibi Chen, Eunseok Lee, Anantha P. Chandrakasan, and Ruonan Han Massachusetts Institute of Technology, USA Email: mingran@mit.edu; ruonan@mit.edu

Abstract — This paper presents the first fully integrated on-chip sub-THz retro-backscatter CMOS circuit, operating at 263 GHz. Using the Van Atta reflector principle and a signal swapping and mode-conversion electromagnetic structure, the design achieves retro-directive operation with a 3-dB angle availability of 105°/82°. Fabricated in an Intel-16 CMOS process, the prototype demonstrates BPSK modulation over an input power range of -7 dBm to -13.9 dBm at 263 GHz, exhibiting a measured conversion loss of 12 dB and capability of Mbps-level data rate at 5-cm reader-to-chip distance. These findings validate a low-cost, low-power, wide-angle THz retro-backscatter solution, improving the performance and practicality of ultra-miniaturized tag applications.

Keywords — retro backscatter communication, RFID, terahertz, CMOS, Van Atta array

#### I. INTRODUCTION

Backscattering enables devices to transmit data through the reflection of interrogation signals, which is a promising, power-efficient communication technique in Internet of things (IoT) and radio-frequency identification (RFID) applications. However, the drawback of backscattering is the significant path loss, as the signal must traverse the propagation channel twice. This limitation becomes more pronounced at higher frequencies. Previous studies have demonstrated the feasibility of realizing THz backscattering on silicon [1], [2] for package-less RFID applications, which is called THzID. Due to the small wavelength at THz frequencies, the antenna and ID size can be reduced to a compact footprint, making the THzID platform suitable for the authentication and tracking of both critical, small components (e.g., dental implants, medical devices, semiconductor chips), as well as high-value fashion items (e.g., luxury eyewear or jewelry) where traditional MHz-to-GHz RFID tags are cumbersome or aesthetically undesirable (Fig. 1). One solution to mitigate the path loss is to adopt multi-antenna arrays; however, this approach severely reduces the reader-to-tag angle availability, defined as the angle range of incident wave that has <3 dB degradation of the reader-received power. In [1], an on-THzID beam searching and steering scheme is adopted to alleviate this problem, but it adds more complexity in the circuit implementation and communication protocols.

Alternatively, retro-reflective antenna arrays [3] merit special consideration. These arrays possess a unique property known as retro-reflectivity, reflecting incoming signals back toward the source without explicit knowledge of the source location. This characteristic allows multi-antenna gains to be effectively leveraged in backscattering systems with reduced penalty of angle availability. However,

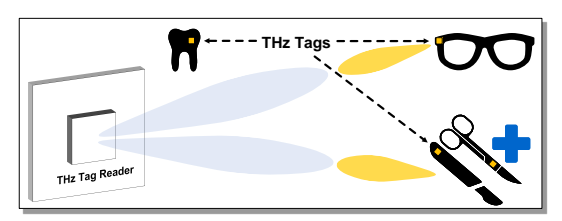


Fig. 1. Potential applications of the fully integrated THz retro-backscatter chip.

developing and implementing low-cost, low-power THz retro-backscatter devices capable of establishing directional links remains a major challenge. A recent work in [4] leveraged the fundamental characteristics of leaky-wave devices to realize directional backscatter. However, that solution relies on multiple dual-slot leaky waveguides and embedded mirrors in a waveguide cavity, which is costly and incompatible with CMOS processes, thus preventing monolithic on-chip integration. Lastly, it is noteworthy that at sub-THz frequencies, conventional implementations of the signal-swapping scheme (to be discussed next) for retro-reflection also encounter problems of inteference among signals in different antennas.

In this paper, we present, for the first time, a fully integrated on-chip terahertz retro-backscatter CMOS chip operating at 263 GHz. This solution improves the 3-dB reading angle availability of a two-antenna backscatter scheme to  $105^{\circ}/82^{\circ}$ . In the meantime, through a multi-functional on-chip electromagnetic structure and a FinFET CMOS technology, a THzID modulation conversion loss of 12 dB, 6-dB lower than that in [1], is achieved.

# II. SYSTEM ARCHITECTURE AND OPERATION PRINCIPLE

In this work, we adopt the concept of the Van Atta reflector [3] that is typically used for retro-backscattering. As illustrated on the right side of Fig. 2, the two antennas in the Van Atta array swap their received signals and then re-radiate. Assuming a plane wavefront arriving with angle  $\theta_1$  and the distance bewteen  $ANT_1$  and  $ANT_2$  is d, due to the signal-swapping, the round trips of the waves through both antennas include the same path length of  $d \cdot \sin \theta$ ; hence, along the direction towards the original source of radiation, the wavefronts eventually carry identical phase and the corresponding interference causes the backscattered beam to propagate towards the source of radiation (i.e. retro-backscattering). In this section, detailed implementations of both such an operation and a BPSK modulation are presented.

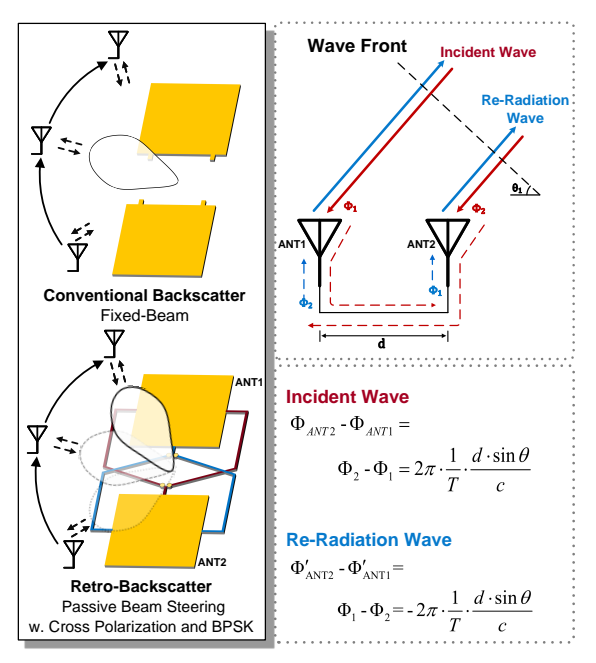


Fig. 2. Implementation principle of the adopted 2-element Van Atta array [3].

## A. Overview of the Cross-Polarization Backscatter Circuit

The system, shown in Fig. 3, comprises an on-chip THz retro-backscatter two-element patch antenna array and the associated on-chip control circuitry. In particular, an electromagnetic structure consisting of two switch pairs connects the two antennas, and its operation principles are excplained in Fig. 4. To minimize the interference between the TX and RX modes at the reader side, the chip architecture utilizes two orthogonal modes ( $TM_{100}$  and  $TM_{010}$ ) of a patch antenna for simultaneous transmission and reception. Such cross-polarization backscattering normally requires two separate signal paths connecting the horizontal edge of one square-shape patch antenna to the vertical edge of another patch, respectively. That, however, leads to excessively long interconnects, leading to high conversion loss. If phase modulation, such as BPSK modulation is needed for uplink, more interconnects are required to route the signals to opposite sides of the second patch for phase inversion in the backscattered wave, further adding loss and complexity. To address those issues, we adopt a multi-function electromagnetic structure, which simultaneously carries the  $ANT_1$ -to- $ANT_2$  signal and  $ANT_2$ -to- $ANT_1$  signal. In different parts of the structure, these two signals are converted to different modes (common-mode and differential mode) so that they co-exist without interference. The differential mode also facilitate BPSK modulation.

## B. Proposed Multi-Modal Electromagnetic Switch Pairs

Shown in Fig. 4 and Fig. 5, the  $TM_{010}$  mode corresponding to common-mode (CM) signaling of two feeds of  $ANT_1$  is used to receive waves with polarization in the vertical direction; and the  $TM_{100}$  mode corresponding to differential-mode (DM) signaling of the feeds of  $ANT_2$  is

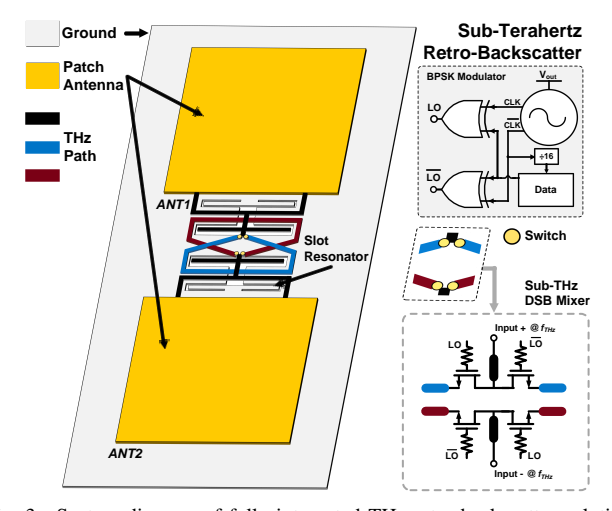


Fig. 3. System diagram of fully integrated THz retro-backscatter solution

used to transmit waves with polarization in the horizontal direction. In Fig. 4, from the two ports of the antenna at the top in the reception mode, the received common-mode waves first meet in the center, and with the slot in the ground, the wave continues propagate downward in the form of quasi-TEM wave (or CPW mode wave). Note that the wave does not form any field inside the vertical folded slot lines (Fig. 4(a)), because the corresponding TM mode with symmetrical E-field distribution is not supported by the vertical slot. Next, controlled by the FinFET switch pair, the wave is re-directed to one of the microstrip lines in the center portion of the EM structure (colored in blue). As the microstrip line spans across the ground vertical slot in the lower half of the EM structure, it excites the quasi-TE wave (with asymmetric E-field distribution, see Fig. 4(a)), and ultimately drives the ports of  $ANT_2$  at the bottom with opposite phases (i.e. differential mode). Similarly, through the same structure and mode-conversion scheme (now common mode at the bottom to differential mode at the top), the incoming wave is also received by  $ANT_2$  and re-radiated by  $ANT_1$ , enabling Van Atta retro-backscattering.

Through the presented structure, only the antenna feeds on the two adjacent edges of the antennas are used, and the swapped signals travel across a short distance between the two edges, reducing power loss. Shown in Fig. 3(b), the switched re-direction of the signal to the left or right of the microstrip line readily enables BPSK modulation. The aforementioned problems are hence solved.

# C. Other Circuit Details

Shown in Fig. 3(c), the length of each branch of the microstrip line is set to quarter-wavelength so that the open circuit formed by the "OFF" switch creates a virtual short between the microstrip line and the ground edge below. Such a short circuit connection guides the forward current inside the microstrip to the ground slot edge, so that it continues propagating downwards, and the return current propagates along the other edge of the ground slot. As is shown in

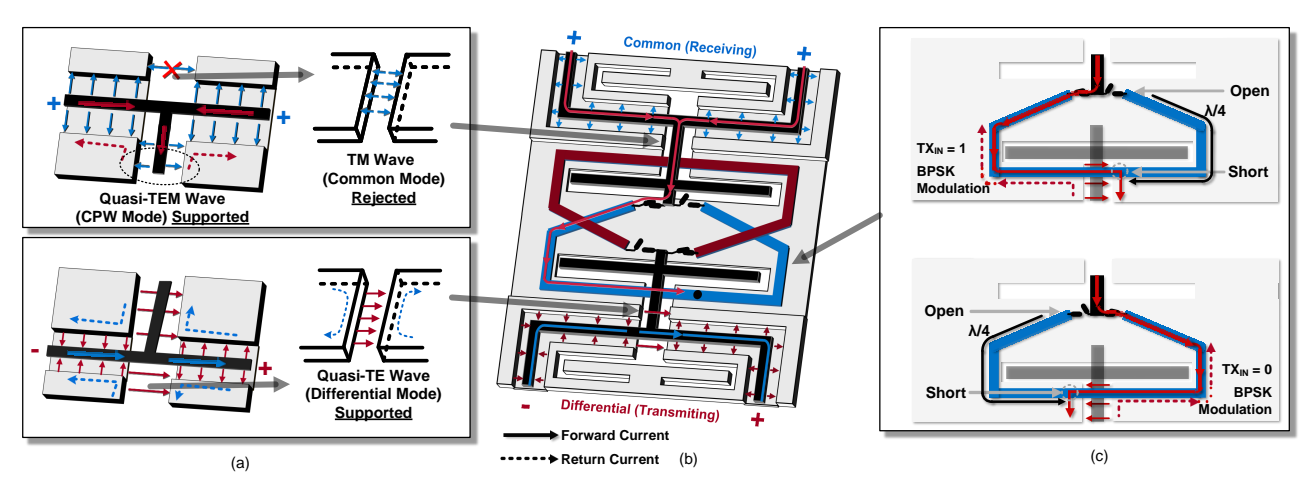


Fig. 4. Architecture of the proposed retro-backscatter BPSK modulator and its equivalent circuit.

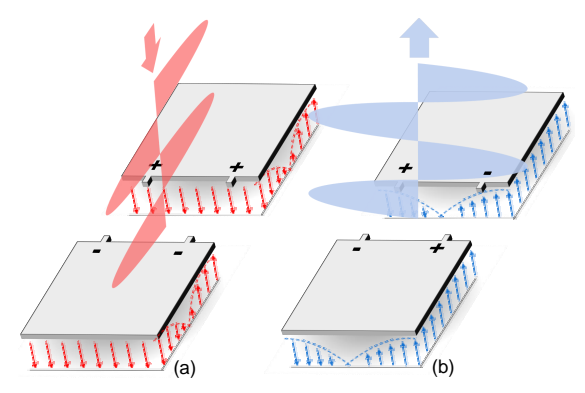


Fig. 5. Radiation pattern of multi-port patch antenna with excited (a)  $TM_{010}$  for receiving and (b)  $TM_{100}$  for re-radiation.

Fig. 6(a), the wave in the slot is then converted to differential signals in the microstrip pair at the bottom. In addition to the built-in BPSK function, another two advantages of the above CM-to-DM conversion is the small insertion loss (0.57 dB in the simulation in Fig. 6)(c) and the negligible amplitude and phase differences between the two differential outputs (Fig. 6)(b)) since any common-mode component is fully rejected during the microstrip-to-slot mode conversion.

Lastly, to close the end of each vertical ground slot, a pair of folded slot line resonators are used (Fig. 7). Since the directions of the E-fields inside adjacent folded sections are opposite, the radiation from these slots is hence suppressed and the resonator loss is reduced. In addition, as described before (Fig. 4(a)), common-mode signals do not propagate into the slot resonators at the top and bottom of the electromagnetic structure, which further reduce the loss. Fig. 8(a) presents the simulated spectrum of our BPSK modulation scheme. With a -10-dBm, 263-GHz carrier input, the retro-backscatter circuit achieves a simulated conversion loss of 10.2 dB (antenna radiation loss not included). The LO signals, generated by an on-chip ring oscillator at 2.5 MHz, provide even-order harmonic suppression and an 11-dB suppression of the third-order harmonic.

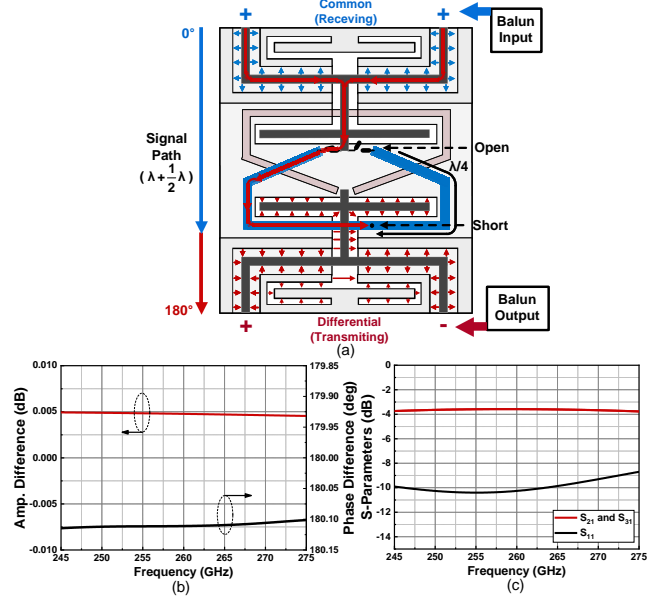


Fig. 6. Slot balun: (a) E-field distribution; (b) simulated amplitude and phase difference between differential outputs; (c) simulated S-parameters.

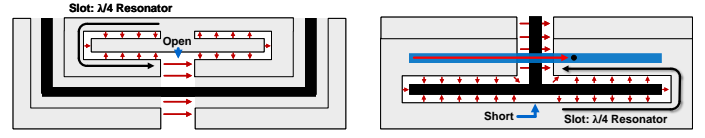


Fig. 7. E-field distribution of the quarter-wavelength resonators.

## III. PERFORMANCE AND EXPERIMENTAL RESULTS

The chip is fabricated using an Intel-16 CMOS process. The measured DC power, consumed by the on-chip MHz oscillator and modulator, is 0.95  $\mu$ W. The measurement setup is shown in Fig. 9, which uses two WR-3.4 horn antennas with orthogonal polarizations for the transmission and receiving modes of the reader. An amplifier multiplier chain (AMC) converts a 10.9375-GHz input to a 262.5-GHz output. The conversion loss of the chip was determined using

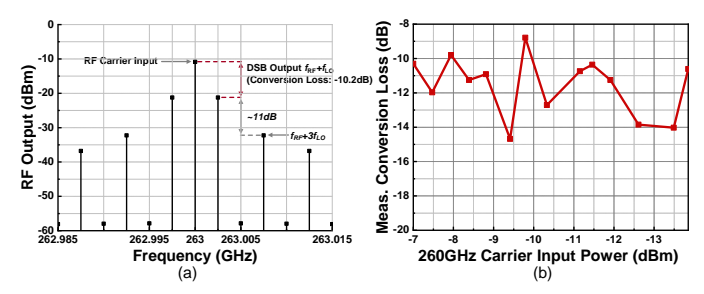


Fig. 8. (a) Simulated conversion loss. (b) Measured conversion loss under varying input power. Input power higher than -8.5 dBm is achieved by decreasing the chip-to-reader distance below 5 cm. The antenna radiation efficiencies are not included in both plots.

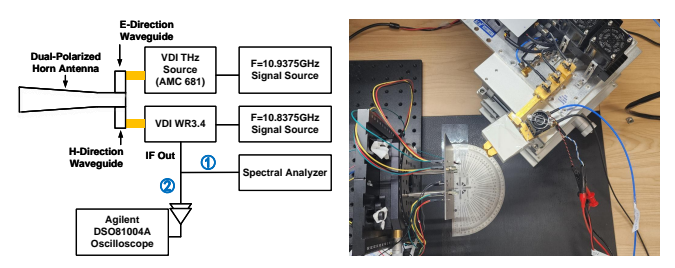


Fig. 9. Measurement setup of the retro-backscatter chip

the Friis equation. At a 5-cm far-field distance, the reader transmits up to 19.7 dBm with a 25-dBi antenna gain at 263 GHz, while the simulated gain of the on-chip antenna is 2 dBi. The reader measures the backscattered signal power, resulting in the conversion loss value after comparing with the calculated received signal power. Fig. 8(b) shows the measured conversion loss of our chip, demonstrating that for input signal power ranging from -7 dBm to -13.9 dBm, the conversion loss is averaged at 12 dB.

The measured down-converted spectrum in Fig. 10(a) shows a pair of strong sideband tones with 36-dB SNR at 1-kHz resolution bandwidth. That indicates that an uplink data rate at Mbps level is supported by the setup. Lastly, Fig. 11 presents the reader-received power at varying reader-chip deviation angles in the measurement. As a reference,

Table 1. Comparison with Other State-of-the-Art THz Backscatter Chips

	This Work	[1]	[2]
Process	Intel-16 CMOS	65nm CMOS	65nm CMOS
Carrier Freq. (GHz)	260	260	260
Modulation	BPSK	OOK	BPSK
Antenna Count	2x1	2x2	1
DC Power (μW)	0.95	13	0.92
Reading Angle Availibility	105°/82°	20°/20°	N/A
SNR (dB)@RBW (Hz)	36*@1000	36*@1000	22*@1
Modulation Conv. Loss (dB)	12 <sup>(a)</sup>	18 <sup>(b)</sup>	N/A <sup>(c)</sup>
Beam Steering?	Yes (Passive)	Yes (Phas. Ctrl.)	No
Active Chip Area (mm <sup>2</sup> )	0.32	1.5 <sup>(d)</sup>	$3.5^{(d)}$

<sup>\*</sup>These SNR measurements were taken with a 260-GHz source with 19.7-dBm radiated power, 25-dBi horn antenna gain and 5-cm distance. (a) Measured results; (b) Simulated results; (c) The conversion loss of the THz PUF chip is dependent on the chip-to-object attachment interface; (d) The chips also include other components for photovoltaic energy harvesting, encryption and PUF key generation.

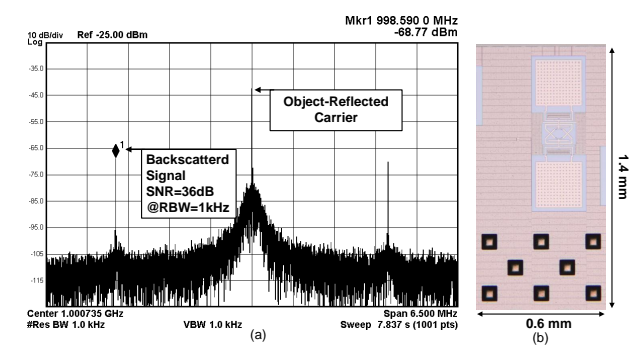


Fig. 10. (a) Measured spectrum of the retro-backscattered uplink beam. (b) Die photo of the work.

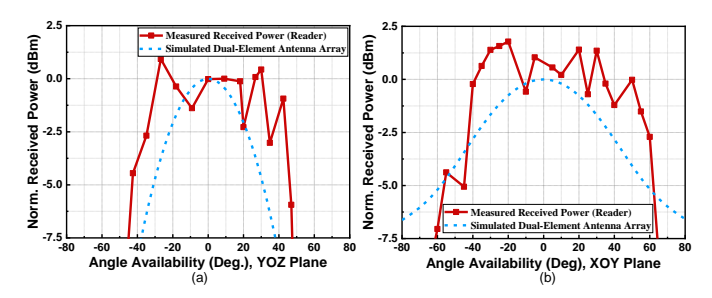


Fig. 11. Measured chip responses to varying reader-chip deviation angles.

the simulated angle responses of a normal two-antenna array are also given, which is narrow (48°) in the plane where two antennas interfere (Fig. 11(a)). Due to the retro-backscattering, the 3-dB angle availability increases to 82° in the measurement. In the other plane (Fig. 11(b)), the measured angle availability of 105° is similar to that of simulation. The die photo of the chip is given in Fig. 10(b).

#### IV. CONCLUSION

In Table 1, this work is compared with the previous THzIDs with the same carrier frequency and testing setup. Due to the retro-backscatter operation, an improvedreading angle availability is achieved, allowing for more convenient and reliable user scenario. In addition, benefiting from our multi-modal electromagnetic signal-swapping structure, as well as a more advanced CMOS node, a lower modulation conversion loss of 12 dB is achieved.

## ACKNOWLEDGMENT

The authors thank the Intel University Shuttle Program and MIT Center of Integrated Circuits and Systems for their supports.

#### REFERENCES

- M. I. Ibrahim et al., "THzID: A 1.6mm<sup>2</sup> Package-Less Cryptographic Identification Tag with Backscattering and Beam-Steering at 260GHz," in ISSCC, 2020, pp. 454

  –456.
- [2] E. Lee et al., "A Packageless Anti-Tampering Tag Utilizing Unclonable Sub-THz Wave Scattering at the Chip-Item Interface," in ISSCC, 2024, pp. 226–228.
- [3] C. Pon, "Retrodirective Array Using the Heterodyne Technique," *IEEE Trans. Antennas Propag.*, pp. 176–180, 1964.
- [4] A. Kludze et al., "A Frequency-Agile Retrodirective Tag for Large-Scale Sub-Terahertz Data Backscattering," Nat. Commun., no. 1, p. 8756, 2024.